

# DualGAN: Unsupervised Dual Learning for Image-to-Image Translation

Zili Yi <sup>1,2</sup>, Hao (Richard) Zhang<sup>2</sup>, Ping Tan <sup>2</sup>, and Minglun Gong<sup>1</sup>

<sup>1</sup>Memorial University of Newfoundland

<sup>2</sup>Simon Fraser University

## Abstract

Using conditional Generative Adversarial Network (conditional GAN) for cross-domain image-to-image translation has achieved significant improvements in the past year [6, 7, 18, 9, 3, 15]. Depending on the degree of task complexity, thousands or even millions of labeled image pairs are needed to train conditional GANs. However, human labeling is very expensive and sometimes impractical. Inspired by the success of dual learning paradigm in natural language translation [20], we develop a novel dual-GAN mechanism, which enables image translators to be trained from two sets of unlabeled images each representing a domain. In our architecture, the primal GAN learns to translate images from domain  $U$  to those in domain  $V$ , while the dual GAN learns to convert images from  $V$  to  $U$ . The closed loop made by the primal and dual tasks allows images from either domain to be translated and then reconstructed. Hence a loss function that accounts for the reconstruction error of images can be used to train the translation models. Experiments on multiple image translation tasks with unlabeled data show considerable performance gain of our dual-GAN architecture over a single GAN. For some tasks, our model can even achieve comparable or slightly better results to conditional GAN trained on fully labeled data.

## 1. Introduction

Many image processing and computer vision tasks, e.g., edge detection, image segmentation, stylization, and abstraction, can be posed as image-to-image translation problems [3], which convert one visual representation of an object or scene into another. Conventionally, these tasks have been tackled separately due to their intrinsic disparities [6, 7, 18, 9, 3, 15]. It is not until the past two years that general-purpose and end-to-end deep learning frameworks, most notably those utilizing fully convolutional net-

works (FCNs) [8] and conditional generative adversarial nets (cGANs) [3], have been developed to enable a *unified* treatment of these tasks.

Up to date, these general-purpose methods have all been supervised and trained with a large number of *labeled* and *matching* image pairs. In practice however, acquiring such training data can be time-consuming (e.g., with pixelwise or patchwise labeling) and even unrealistic. For example, while there are plenty of photos or sketches available, photo-sketch image pairs depicting the same persons under the same poses are scarce. In some other situations, such as converting daylight scenes to night scenes, even though labeled and matching image pairs can be obtained with stationary cameras, they are not accurately aligned and may contain slightly different contents.

In this paper, we aim to develop an *unsupervised* learning framework for general-purpose image-to-image translation, which only relies on *unlabeled* image data, such as two sets of photos and sketches for the photo-to-sketch conversion task. The obvious technical challenge is how to train a translator without any data characterizing correct translations. Our approach is inspired by *dual learning* from natural language processing [20]. Dual learning trains two “opposite” language translators (e.g., English-to-French and French-to-English) simultaneously by minimizing the *reconstruction loss* resulting from a *nested* application of the two translators. The two translators represent a primal-dual pair and the nested application forms a closed loop, allowing the application of reinforcement learning. Specifically, the reconstruction loss measured over monolingual data (either English or French) would generate informative feedback to train a bilingual translation model.

Our work develops a dual learning framework for image-to-image translation for the first time and differs from the original NLP dual learning method of Xia et al. [20] in two main aspects. First, the NLP method relied on pre-trained (English and French) language models to indicate how confident the translator outputs are natural sentences in their respective target languages. With general-purpose process-

ing in mind and the realization that such pre-trained models are difficult to obtain for many image translation tasks, our work develops GAN discriminators [2] that are trained adversarially with the translators to capture domain distributions. Hence, we call our learning architecture *DualGAN*. Furthermore, we employ FCNs as translators which naturally accommodate the 2D structure of images, rather than sequence-to-sequence translation models such as LSTM or GUT.

Taking two sets of unlabeled images as input, each representing an image domain, DualGAN simultaneously learns two reliable image translators from one domain to the other and hence can operate on a wide variety of image-to-image translation tasks. Its effectiveness is validated through comparison with both GAN (with an image-conditional generator and the original discriminator) and conditional GAN [3]. The comparison results demonstrate that, for some applications, DualGAN can outperform supervised methods trained on labeled data.

## 2. Related work

### 2.1. Generative adversarial networks (GANs)

Since the seminal work by Goodfellow et al. [2] in 2014, a series of GAN-family methods have been proposed for a wide variety of problems. The original GAN can learn a generator to capture the distribution of real data by introducing an adversarial discriminator that evolves to discriminate between the real data and the fake [2]. Soon after, various conditional GANs (cGAN) have been proposed to condition the image generation on class labels [10], attributes [11, 21], texts [12], and images [6, 7, 18, 9, 3, 15].

Among the image-conditional models, most were developed for specific applications such as super-resolution [6], texture synthesis [7], style transfer from normal maps to images [18], and video prediction [9], whereas few others were aiming for general-purpose processing [3, 15]. The general-purpose solution for image-to-image translation proposed by Isola et al. [3] requires significant number of labeled image pairs. The unsupervised mechanism for cross-domain image conversion presented by Taigman et al. [15] can train an image-conditional generator without paired images, but relies on a sophisticated pre-trained function that maps images from either domain to an intermediate representation, which requires labeled data in other formats. Unlike these methods, our dual-GAN mechanism only requires unlabeled images from two related domains, and it works without any third-party representations acting as bridges between the two. In addition, it trains both primal and dual GANs at the same time, allowing a reconstruction error term being used for generating informative feedback signals. Though our DualGAN adopts the key idea of GANs, which is forcing generated data to comply with the

targeted distribution through a self-evolving discriminator.

### 2.2. Dual learning

Dual learning was first proposed by Xia et al. [20] to reduce the requirement on labeled data in training English-to-French and French-to-English translators. The French-to-English translation is the dual task to English-to-French translation, and they can be trained side-by-side. The key idea of dual learning is to set up a dual-learning game which involves two agents, each of whom only understands one language, and can evaluate how likely the translated are natural sentences in targeted language and to what extent the reconstructed are consistent with the original. Such a mechanism is played alternatively on both sides, allowing translators to be trained from monolingual data only.

Despite of a lack of parallel bilingual data, two types of feedback signals can be generated: the membership score which evaluates the likelihood of the translated texts belonging to the targeted language, and the reconstruction error that measures the disparity between the reconstructed sentences and the original. Both signals are assessed with the assistance of application-specific domain knowledge, i.e., the pre-trained English and French language models.

In our work, we aim for a general-purpose solution for image-to-image conversion and hence do not utilize any domain-specific knowledge or pre-trained domain representations. Instead, we use a domain-adaptive GAN discriminator to evaluate the membership score of translated samples, whereas the reconstruction error is measured as the mean of absolute difference between the reconstructed and original images.

## 3. Method

Assuming that we have two sets of unlabeled images sampled from image domains  $U$  and  $V$ , respectively. The primal task is to learn a generator  $G_A : U \rightarrow V$  that maps image  $u \sim U$  to image  $v \sim V$ , and the dual task is to train a generator  $G_B : V \rightarrow U$ . To realize this, we employ two GANs, the primal GAN and the dual GAN. The primal GAN learns the generator  $G_A$  and a discriminator  $D_A$  that discriminates between  $G_A$ 's fake outputs and the real members of domain  $V$ . Similarly, the dual GAN learns the generator  $G_B$  and a discriminator  $D_B$ . The overall architecture and dataflow are illustrated in Fig. 1.

As shown in Fig. 1, the raw data  $u \sim U$  gets translated to domain  $V$  using  $G_A$ . How well the translation result  $G_A(u, z)$  fits in  $V$  is evaluated by  $D_A$ , where  $z$  is random noise (so is  $z'$  that appears below).  $G_A(u, z)$  is then translated back to domain  $U$  using  $G_B$ , which outputs  $G_B(G_A(u, z), z')$  as the reconstructed version of  $u$ . Similarly,  $v \sim V$  is translated to  $U$  as  $G_B(v, z')$  and then reconstructed as  $G_A(G_B(v, z'), z)$ . The discriminator  $D_A$  is trained with  $v$  as positive samples and  $G_A(u, z)$  as negative

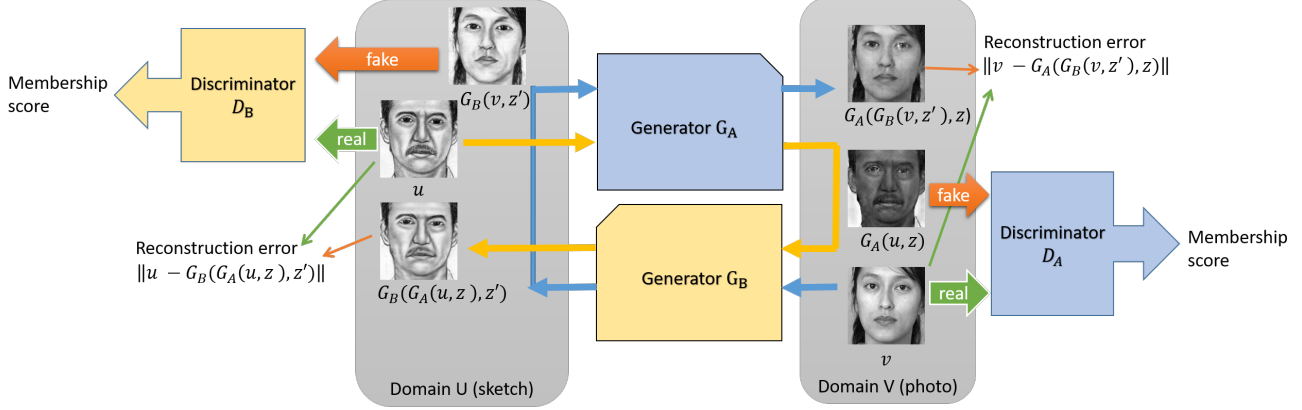


Figure 1: Architecture and dataflow chart of the dual learning mechanism.

examples, whereas  $D_B$  takes  $u$  as positive and  $G_B(v, z')$  as negative. Generators  $G_A$  and  $G_B$  are optimized to emulate “fake” outputs to blind the corresponding discriminators  $D_A$  and  $D_B$ , as well as to minimize the reconstruction loss  $\|G_A(G_B(v, z'), z) - v\|$  and  $\|G_B(G_A(u, z), z') - u\|$ .

### 3.1. Objective

As in the traditional GAN, the objective of discriminators is to discriminate the generated fake samples from the real. Nevertheless, here we use the loss format advocated by Wasserstein GAN (WGAN) [1] rather than the sigmoid cross-entropy loss used in the original GAN [2]. It is proven that the former performs better in terms of generator convergence and sample quality, as well as improves the stability of the optimization process [1]. The corresponding loss functions used in  $D_A$  and  $D_B$  are defined as:

$$l_A^d(u, v) = D_A(G_A(u, z)) - D_A(v), \quad (1)$$

$$l_B^d(u, v) = D_B(G_B(v, z')) - D_B(u) \quad (2)$$

where  $u \sim U$  and  $v \sim V$ .

The same loss function is used for both generators  $G_A$  and  $G_B$  as they share the same objective. Previous approaches for conditional image synthesis have found it beneficial to replace  $L2$  distance with  $L1$ , since  $L2$  often leads to blurriness [5, 20]. Hence, here we use  $L1$  distance to measure recovery error, which is added to the GAN objective that forces the translated samples to obey domain distribution; see Eq. 3.

$$l^g(u, v) = \lambda_U \|u - G_B(G_A(u, z), z')\| + \lambda_V \|v - G_A(G_B(v, z'), z)\| - D_A(G_B(v, z')) - D_B(G_A(u, z)), \quad (3)$$

where  $u \sim U$ ,  $v \sim V$  and  $\lambda_U$ ,  $\lambda_V$  are two constant parameters. Depending on the application,  $\lambda_U$  and  $\lambda_V$  are typically

set to  $100.0 \sim 1,000.0$ . If  $U$  are natural images and  $V$  are not (e.g., aerial photo-maps), we find it more effective to use smaller  $\lambda_U$  than  $\lambda_V$ .

### 3.2. Network Configuration

We use identical network architecture for  $G_A$  and  $G_B$ . The generator is configured with equal number of down-sampling layers (pooling layers) and up-sampling layers. In addition, we configure the generator with skip connections between mirrored downsampling layers and up-sampling layers as in [13, 3], making it a U-shaped net. Such a design enables low-level information to be shared between the input and output, which is beneficial because many image translation problems implicitly demand alignment between input and output structure (e.g., objects, shapes, edges, textures, clutters, etc.). Without the skip layers, information of all levels has to pass through the bottleneck, typically causing significant loss of high-frequency information. Furthermore, similar to [3], we did not explicitly provide the noise vectors  $z, z'$ . They are provided only in the form of dropout and applied on several layers of our generators at both training and test time: please see [3] for more details.

For discriminators, we employ the Markovian Patch-GAN architecture as explored in [7], which assumes independence between pixels distanced beyond specific patch size and models images only at patch level rather than at full image size. Such a configuration is effective in capturing local high-frequency features such as texture and style, but less so in modeling global distribution. It satisfies our needs, since the recovery loss encourages preservation of global and low-frequency information and the discriminators are designated to capture local high-frequency information. The effectiveness of this configuration has been verified on various image translation tasks [20]. Similar to [20], we run this discriminator convolutionally across the im-

age, averaging all responses to provide the ultimate output. An extra advantage of such a configuration is that it requires fewer parameters, runs faster, and has no constraints on size of input images.

### 3.3. Training procedure

To optimize our networks, we follow the training procedure proposed in WGAN [1]: see Alg. 1. We train the discriminators  $n_{critic}$  steps, then one step on generators. We use mini-batch Stochastic Gradient Descent and apply the RMSProp solver, as momentum based methods like Adam occasionally cause instability [1], and RMSProp is known to perform well even on highly non-stationary problems [16, 1]. We typically set the number of critic iterations per generator iteration  $n_{critic}$  to 2-4 and assign batch size to 1-4, noting little influences on effectiveness in experiments. The clipping parameter  $c$  is normally set to  $0.01 \sim 0.1$ , varying by application.

---

#### Algorithm 1 DualGAN training procedure

---

**Require:** Image set  $U$ , image set  $V$ , GAN  $A$  with generator parameters  $\theta_A$  and discriminator parameters  $\omega_A$ , GAN  $B$  with generator parameters  $\theta_B$  and discriminator parameters  $\omega_B$ , clipping parameter  $c$ , batch size  $m$ ,  $n_{critic}$

- 1: Randomly initialize  $\omega_i, \theta_i, i \in \{A, B\}$
- 2: **repeat**
- 3:   **for**  $t = 1, \dots, n_{critic}$  **do**
- 4:     sample images  $\{u^{(k)}\}_{k=1}^m \sim U, \{v^{(k)}\}_{k=1}^m \sim V$
- 5:     update  $\omega_A$  to minimize  $\frac{1}{m} \sum_{k=1}^m l_A^d(u^{(k)}, v^{(k)})$
- 6:     update  $\omega_B$  to minimize  $\frac{1}{m} \sum_{k=1}^m l_B^d(u^{(k)}, v^{(k)})$
- 7:      $clip(\omega_A, -c, c), clip(\omega_B, -c, c)$
- 8:   **end for**
- 9:   sample images  $\{u^{(k)}\}_{k=1}^m \sim U, \{v^{(k)}\}_{k=1}^m \sim V$
- 10:   update  $\theta_A, \theta_B$  to minimize  $\frac{1}{m} \sum_{k=1}^m l^g(u^{(k)}, v^{(k)})$
- 11: **until** convergence

---

For traditional GAN, the training procedure needs to carefully balance between the generator and the discriminator. This is because, as the discriminator gets better, the sigmoid cross-entropy loss is locally saturated and leads to vanishing gradients. Unlike traditional GAN, Wasserstein loss is differentiable almost everywhere, resulting a better discriminator. For each iteration, The generators are not trained until the discriminators have been trained for  $n_{critic}$  steps. Such a procedure enables the discriminators to provide more reliable gradient information [1].

## 4. Experimental Results and Evaluation

To explore the generality of DualGAN, we test the method on a wide variety of image-to-image mapping tasks,

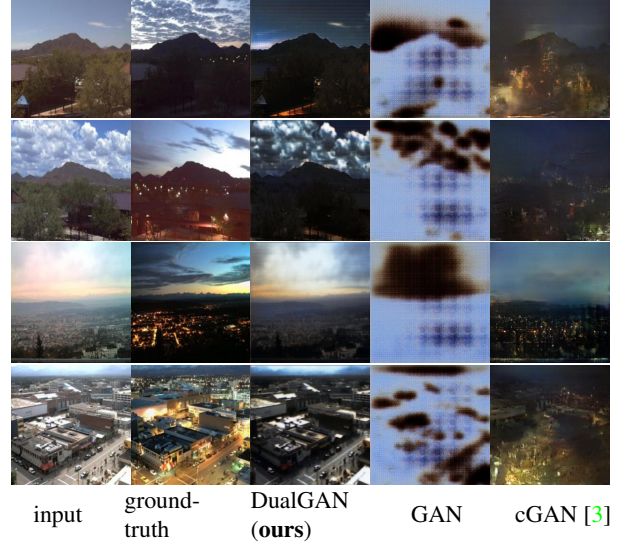


Figure 2: Results for day→night translation. cGAN [3] is trained with labeled data, whereas DualGAN and GAN are trained in an unsupervised way. DualGAN successfully emulates the night scenes while preserves the texture of the inputs; see the differences on clouds between our results and the ground truth. In comparison, results of cGAN and GAN contain much less details.

including photo-sketch conversion, label-image translation, and artistic stylization of images.

In order to compare our unsupervised DualGAN with GAN and cGAN [3]. Four labeled datasets are used: PHOTO-SKETCH [19, 22], DAY-NIGHT [4], LABEL-FACADES [17], and AERIAL-MAPS, which is directly captured from google map [3]. These datasets consist of image pairs that map images from one domain to the other and hence can be used for supervised learning. However, it is worth noting that none of these datasets guarantees accurate feature alignment at pixel level. For example, the sketch images in SKETCH-PHOTO dataset are drawn by artists and hence do not accurately align with the corresponding photos, moving objects and road lights often show up in the DAY-NIGHT dataset, and the labels in LABEL-FACADES dataset are not always precise. This highlights the difficulties of obtaining high quality matching image pairs.

Our method enables us to make use of abundant unlabeled resources from the Web. Hence, two additional unlabeled datasets are also used for experiments. The MATERIAL dataset includes images of objects made of different materials, e.g., stone, metal, plastic, fabric, and wood. These images were manually selected from Flickr and cover a variety of illumination conditions, compositions, colors, texture and material sub-types [14]. This dataset is initially



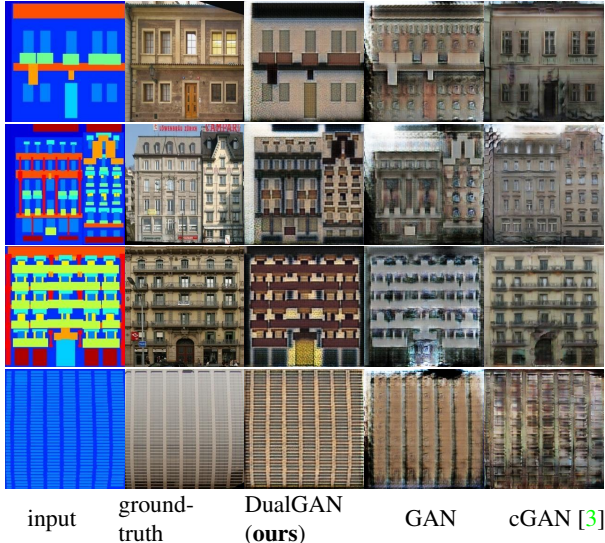


Figure 3: Results for architecture label→photo translation. DualGAN faithfully preserves the structures in the labeling image, even though some labels do not match well with the corresponding photos; see for example the first two images in top row. In comparison, results of GAN and cGAN contain many artifacts. In areas that labels and photos are commonly misaligned, cGAN often yields blurry output (e.g., the roof in 2nd row and the entrance in 3rd row).

used for material recognition, but is used here for material-transfer. The OIL-CHINESE painting dataset includes artistic paintings of two disparate styles: oil paintings and Chinese paintings. All images are crawled from search engines, which contains images with various quality, formats, and size. We reformat, crop and resize the images for training and evaluation. In both of the above two datasets, no correspondence information is available between images from different domains.

## 5. Qualitative evaluation

Using the four labeled datasets, we first compare our approach with both GAN and cGAN [3] on the following image translation tasks: day→night (Figure 2), architectural labels↔photo (Figure 3 and 10), face photo↔sketch (Figure 4 and 5), and map↔aerial photo (Figure 8 and 9).

In all these tasks, the cGAN is trained with labeled data. Here we employ the model and codes provided in [3] and choose the optimal loss function for each task:  $L1$  loss for facades→label and  $L1 + cGAN$  loss for other tasks (please see [3] for more details). In comparison, DualGAN and GAN are trained in an unsupervised way. That is, we unbind the image pairs and then reshuffle the data. The results of GAN are generated using our approach by setting

$\lambda_U = \lambda_V = 0.0$  in eq. 3, noting that this GAN is different from the original GAN model[2] as it employs a conditional generator.

All three models are trained on the same training datasets and tested on novel data that does not overlap the training datasets. All the training are carried on a single GeForce GTX Titan X GPU. At test time, all models run in well under a second on this GPU.

Compared to GAN, in almost all cases, DualGAN produces results that are less blurry, contain fewer artifacts, better preserve the structures of the inputs, and capture the features (e.g., texture, color, style) of target domain. We attribute the improvement to the additional reconstruction loss, which forces the inputs to be reconstructable from outputs through the dual generator and strengthens feedback signals that encodes the targeted distribution.

In many cases, our results also compare favorably over the ones obtained by cGAN in terms of sharpness and faithfulness to input images; see Figures 2, 3, 4, 5, and 8. This is encouraging as the latter approach utilizes additional image and pixel correspondence information. Nevertheless, when the tasks are translating between photos and semantic-based labels, such as map↔aerial and label↔facades, it is often impossible to infer the correspondences between pixel colors and labels based on targeted distribution alone. As a result, DualGAN may map pixels to wrong labels (see Figure 9 and 10) or labels to wrong colors/textures (see Figures 3 and 8).

Figures 6 and 7 further show the image translation results obtained using the two unlabeled datasets, including: oil painting↔Chinese painting, plastic→metal, metal→stone, leather→fabric, and wood↔plastic. They show that visually convincing images are generated even though no corresponding images can be found in the target domains. The results generally contain less artifacts than those of GAN as well.

### 5.1. Quantitative evaluation

In order to quantitatively evaluate our method, we set up two user-study tasks through Amazon Mechanical Turk (AMT). The “material perceptual” test is used to evaluate the material transfer results, in which we mix the outputs of all material transfer tasks and let the turkers to choose the best match based on which material they believe the objects in the image are made of. We have a total of 176 output images, with each image evaluated by three turkers. The output image is rated as success if at least one turker selects the target material type. The success rates of various material transfer results using different approaches are summarized in Table. 1. It shows that DualGAN outperforms GAN by a large margin.

In addition, we run AMT “realness score” evaluation for sketch→photo, label map→facades, maps→aerial photo,

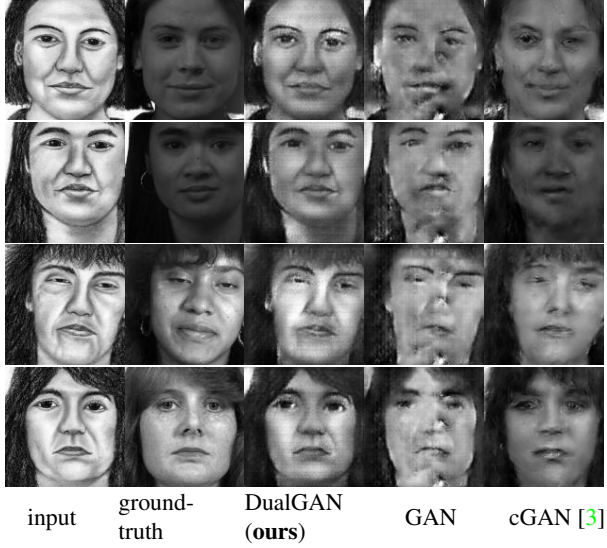


Figure 4: Results for photo→sketch translation. Results of DualGAN are generally sharper than those of cGAN, even though the former is trained using unlabeled data, whereas the latter makes use of labeled data.

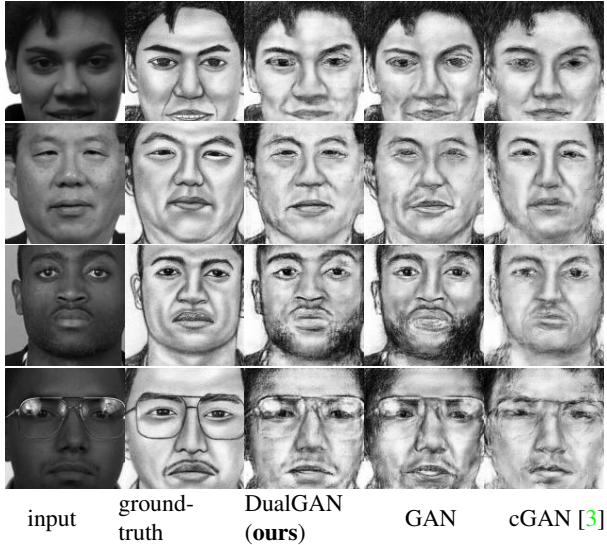


Figure 5: Results for sketch→photo translation. More artifacts and blurriness are shown up in results generated by GAN and cGAN than in ours.

and day→night translation results. To eliminate potential bias, for each of the four evaluations, we randomly shuffle real photos and outputs of all three approaches before showing them to turkers. Each image is shown to 3 turkers, who are asked to score the image based on to what extent the

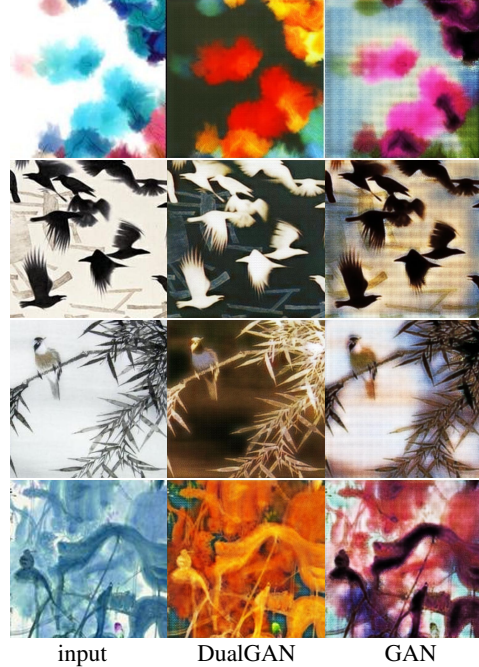


Figure 6: Experimental results for Chinese painting→oil painting task. The background grids shown in the GAN results imply that the outputs of GAN are not as stable as those of DualGAN.

Task	DualGAN	GAN
plastic→wood	1/11	0/11
wood→plastic	1/11	0/11
metal→stone	2/11	1/11
stone→metal	2/11	0/11
leather→fabric	4/11	2/11
fabric→leather	2/11	1/11
plastic→metal	6/11	3/11
metal→plastic	1/11	1/11

Table 1: Success rates of various material transfer tasks based on the AMT “material perceptual” test. There are 11 images in each set of transfer result. As shown in the table, the proposed dual learning mechanism noticeably improves the success rates of material transfer tasks over GAN.

synthesized photo looks real. The “realness” score ranges from 0 (totally missing), 1 (bad), 2 (acceptable), 3 (good) to 4 (compelling). The average score of different approaches on various tasks are then computed and shown in Table. 2. The results show that DualGAN defeats GAN on all tasks and outperforms cGAN on two tasks as well. This indicates that cGAN has little tolerance to misalignment and incon-



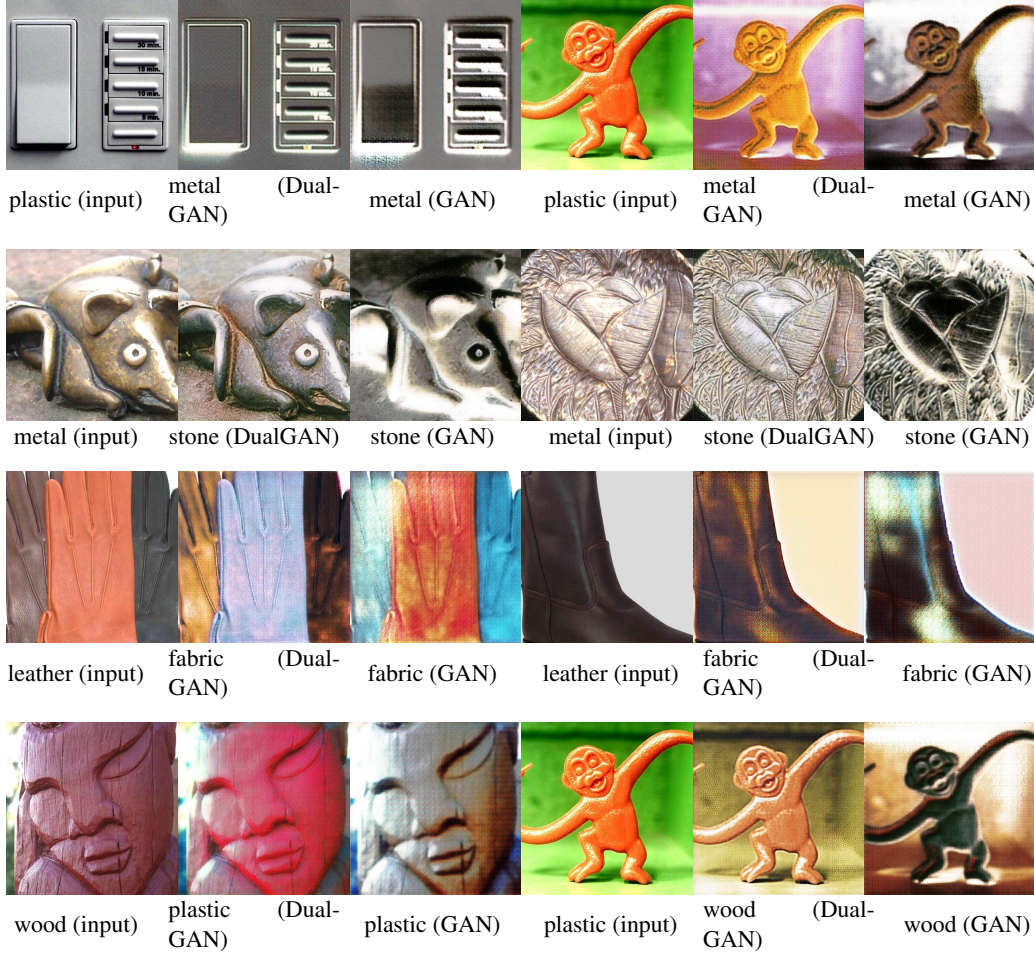


Figure 7: Experimental results for various material-transfer tasks: from top to bottom, plastic→metal, metal→stone, leather→fabric, plastic↔wood.

sistency between image pairs, but the additional correspondence information does help it to correctly map labels to colors and textures.

Finally, we compute the segmentation accuracy for facades→label and aerial→maps tasks: see Table 3 and 4. The comparison shows that DualGAN is outperformed by cGAN. This is expected as it is hard to infer proper labeling without correspondence information.

## 6. Conclusion

We propose a novel unsupervised dual learning framework for general-purpose image-to-image translation. The unsupervised feature enables many more real world applications. Experimental results suggest that our DualGAN mechanism can significantly improve the outputs of GAN for various image-to-image translation tasks. With unlabeled data only, DualGAN can generate comparable or even

better outputs than conditional GAN [3] that can only be trained with labeled data.

On the other hand, our method is outperformed by conditional GAN [3] in certain applications that involves semantic-based labels. This is due to the lack of pixel and label correspondence information, which cannot be inferred from target distribution alone. In the future, we intend to investigate whether this limitation can be tackled with the use of a small number of labeled data for warm start.

## References

- [1] M. Arjovsky, S. Chintala, and L. Bottou. Wasserstein gan. *arXiv preprint arXiv:1701.07875*, 2017. 3, 4
- [2] I. Goodfellow, J. Pouget-Abadie, M. Mirza, B. Xu, D. Warde-Farley, S. Ozair, A. Courville, and Y. Bengio. Generative adversarial nets. In *Advances in neural information processing systems*, pages 2672–2680, 2014. 2, 3, 5



Figure 8: Results for map→aerial photo translation. Without correspondence information, our method maps the orange-colored interstate highways to bright colors of building roofs. Nevertheless, our results are sharper than those of GAN and cGAN.



Figure 9: Results for aerial photo→map translation. DualGAN performs better than GAN, but not as good as cGAN. With additional pixel correspondence information, cGAN performs very well in terms of labeling local roads, but still cannot detect interstate highways.

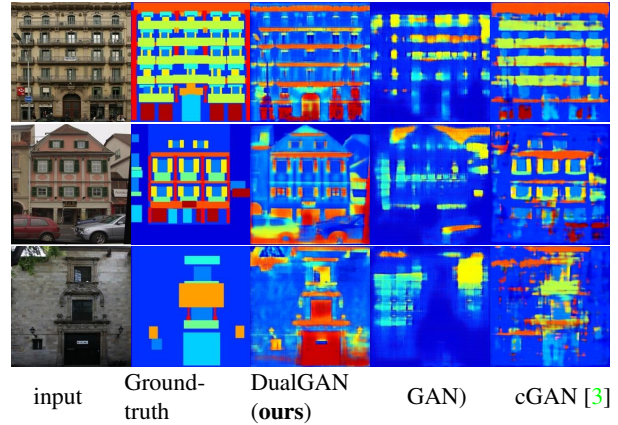


Figure 10: Results for facades→architecture label translation. While cGAN correctly labels various architecture components such as windows, doors, and balconies, the overall label images are not as detailed and structured as our outputs.

task	Avg. 'realness' score			
	DualGAN	cGAN[3]	GAN	ground-truth
sketch → photo	<b>1.78</b>	1.64	1.07	3.61
day → night	<b>2.37</b>	1.93	0.14	3.02
label → facades	1.90	<b>2.65</b>	1.40	3.34
maps → aerial photo	2.55	<b>2.91</b>	1.89	3.17

Table 2: The average AMT “realness” score of outputs of various tasks. The results show that DualGAN outperforms GAN in all tasks. It also outperforms cGAN for sketch→photo and day→night tasks, but still lag behind cGAN for label→facades and maps→aerial tasks. In the latter two tasks, the additional image correspondence information helps cGAN to map labels to proper colors/textures.

	Per-pixel acc.	Per-class acc.	Class IOU
DualGAN	0.27	0.13	0.06
cGAN [3]	<b>0.54</b>	<b>0.33</b>	<b>0.19</b>
GAN	0.22	0.10	0.05

Table 3: The segmentation accuracy for facades → architecture label task. DualGAN outperforms GAN, but is not as accurate as cGAN. This is because, without correspondence information, even if DualGAN segments a region properly, it may not assigning the region with a correct label.

- [3] P. Isola, J.-Y. Zhu, T. Zhou, and A. A. Efros. Image-to-image translation with conditional adversarial networks. *arXiv preprint arXiv:1611.07004*, 2016. [1](#), [2](#), [3](#), [4](#), [5](#), [6](#), [7](#), [8](#), [9](#)
- [4] P.-Y. Laffont, Z. Ren, X. Tao, C. Qian, and J. Hays. Transient attributes for high-level understanding and editing of outdoor scenes. *ACM Transactions on Graphics (TOG)*, 33(4):149, 2014. [4](#)
- [5] A. B. L. Larsen, S. K. Sønderby, H. Larochelle, and O. Winther. Autoencoding beyond pixels using a learned similarity metric. *arXiv preprint arXiv:1512.09300*, 2015. [3](#)



	Per-pixel acc.	Per-class acc.	Class IOU
DualGAN	0.42	0.22	0.09
cGAN [3]	<b>0.70</b>	<b>0.46</b>	<b>0.26</b>
GAN	0.41	0.23	0.09

Table 4: The segmentation accuracy for aerial  $\rightarrow$  maps task. DualGAN again does poorly.

- [6] C. Ledig, L. Theis, F. Huszár, J. Caballero, A. Cunningham, A. Acosta, A. Aitken, A. Tejani, J. Totz, Z. Wang, et al. Photo-realistic single image super-resolution using a generative adversarial network. *arXiv preprint arXiv:1609.04802*, 2016. 1, 2
- [7] C. Li and M. Wand. Precomputed real-time texture synthesis with markovian generative adversarial networks. In *European Conference on Computer Vision*, pages 702–716. Springer, 2016. 1, 2, 3
- [8] J. Long, E. Shelhamer, and T. Darrell. Fully convolutional networks for semantic segmentation. In *Proceedings of the IEEE Conference on Computer Vision and Pattern Recognition*, pages 3431–3440, 2015. 1
- [9] M. Mathieu, C. Couprie, and Y. LeCun. Deep multi-scale video prediction beyond mean square error. *arXiv preprint arXiv:1511.05440*, 2015. 1, 2
- [10] M. Mirza and S. Osindero. Conditional generative adversarial nets. *arXiv preprint arXiv:1411.1784*, 2014. 2
- [11] G. Perarnau, J. van de Weijer, B. Raducanu, and J. M. Álvarez. Invertible conditional gans for image editing. *arXiv preprint arXiv:1611.06355*, 2016. 2
- [12] S. Reed, Z. Akata, X. Yan, L. Logeswaran, B. Schiele, and H. Lee. Generative adversarial text to image synthesis. In *Proceedings of The 33rd International Conference on Machine Learning*, volume 3, 2016. 2
- [13] O. Ronneberger, P. Fischer, and T. Brox. U-net: Convolutional networks for biomedical image segmentation. In *International Conference on Medical Image Computing and Computer-Assisted Intervention*, pages 234–241. Springer, 2015. 3
- [14] L. Sharan, R. Rosenholtz, and E. Adelson. Material perception: What can you see in a brief glance? *Journal of Vision*, 9(8):784–784, 2009. 4
- [15] Y. Taigman, A. Polyak, and L. Wolf. Unsupervised cross-domain image generation. *arXiv preprint arXiv:1611.02200*, 2016. 1, 2
- [16] T. Tieleman and G. Hinton. Lecture 6.5-rmsprop: Divide the gradient by a running average of its recent magnitude. *COURSERA: Neural networks for machine learning*, 4(2), 2012. 4
- [17] R. Tyleček and R. Šára. Spatial pattern templates for recognition of objects with regular structure. In *German Conference on Pattern Recognition*, pages 364–374. Springer, 2013. 4
- [18] X. Wang and A. Gupta. Generative image modeling using style and structure adversarial networks. In *European Conference on Computer Vision*, pages 318–335. Springer, 2016. 1, 2
- [19] X. Wang and X. Tang. Face photo-sketch synthesis and recognition. *IEEE Transactions on Pattern Analysis and Machine Intelligence*, 31(11):1955–1967, 2009. 4
- [20] Y. Xia, D. He, T. Qin, L. Wang, N. Yu, T.-Y. Liu, and W.-Y. Ma. Dual learning for machine translation. *arXiv preprint arXiv:1611.00179*, 2016. 1, 2, 3
- [21] X. Yan, J. Yang, K. Sohn, and H. Lee. Attribute2image: Conditional image generation from visual attributes. In *European Conference on Computer Vision*, pages 776–791. Springer, 2016. 2
- [22] W. Zhang, X. Wang, and X. Tang. Coupled information-theoretic encoding for face photo-sketch recognition. In *Computer Vision and Pattern Recognition (CVPR), 2011 IEEE Conference on*, pages 513–520. IEEE, 2011. 4